ELECTROSTATIC SHIELDING FOR BEARING CURRENT MITIGATION – AN ANALYSIS OF ITS THERMAL IMPACT ON THE MOTOR

Marco T. A. Êvo
Electrical Engineering Department
Federal University of São João del Rei
São João del Rei, MG, 36307-352
Brazil
mtevo@ufsj.edu.br

Arismar M. G. Júnior
Graduate Program in Electrical Engineering
Federal University of Uberlândia
Uberlândia, MG, Brazil
arismarmgj11@gmail.com

Caio Eduardo Silva
Graduate Program in Electrical Engineering
Federal University of Uberlândia
Uberlândia, MG, Brazil
caioeduardo@ufsj.edu.br

Hélder de Paula
Member, IEEE
Faculty of Electrical Engineering
Federal University of Uberlândia
Uberlândia, MG, Brazil
drhelderdepaula@gmail.com

Abstract – This work presents a study on the use of electrostatic shields to reduce bearing currents (both Electrostatic discharge machining and circulating currents), focusing on its thermal impact on the motor operation. 2-D finite element models are utilized to analyze the temperature distribution inside the coil winding slot of motors both with and without shielding. The results show that the shielding device can be used with a negligible influence on the temperature rise inside the slot. In addition, it is demonstrated that for some shield configurations, the stator winding eddy current loss can be attenuated. In such cases, the shield presence can also lead to a temperature reduction in the stator conductors. Furthermore, the developed models can be expanded to be used in the analysis of any other motor equipped with this type of solution, aiding the design and implementation of the shielding device. Keeping in mind that the majority of the motor failures are due to bearing problems, this paper contributes to the industry by addressing issues closely related to the reliability topic, such as solutions to increase the motor availability, which is the very case of the shielding device.

Index Terms — Electrostatic shield, bearing currents, temperature rise, eddy-current loss, induction motor.

I. INTRODUCTION

Although the electric motors can fail for many reasons, it is estimated that almost half of these breakdowns are due to bearing problems [1], which makes this component one of the most critical elements for maintaining normal motor operation [2]. Many factors may cause a bearing failure, such as inappropriate lubrication, excessive loading, high vibration, misalignment and lubricant contamination. However, premature bearing failure can also be ascribed to the presence of electrical currents flowing through the bearings during motor operation. Depending on the amplitude and frequency of occurrence, these currents can cause serious damage to the bearings and increase unwanted motor downtime, as reported in [3] and [4].

The low-frequency bearing currents (or “classical” currents) are related to the line-fed electrical machines, and their resulting problems have been the subject of studies for at least century ([5] and [6]). The most common cause of such bearing current is the presence of asymmetries in the motor magnetic circuit, which results in an induced voltage between the shaft ends [7]. This voltage can thus cause a current circulation that has the machine bearings as part of its circulating path. This type of bearing current is not part of the scope of this work.

On the other hand, the application of any voltage source inverter (VSI) for motor speed and torque control may cause the circulation of some high-frequency bearing currents, also called as inverter-induced bearing currents. Once the inverter output voltage contains a common mode component with variations in steps, the corresponding high dv/dt’s excite all the distributed motor intrinsic capacitances to ground, resulting in high-frequency current circulation. Based on generation mechanism and circulation paths, such currents can be classified as follows: capacitive bearing currents; electrostatic discharge machining (EDM) currents; circulating bearing currents and rotor ground currents. This work focuses on two of the four aforementioned currents: the EDM and the circulating bearing currents.

There are many ways to reduce the inverter-induced bearing currents. Traditional techniques include the motor shaft grounding [8] and the use of insulated bearings [9]. There is also electrostatic shielding, a method not yet commercially available [1], [10] – [14]. It is this method that is the focus of this paper.

Considering the shield application, whether to mitigate the EDMs currents, as shown in [11], or to reduce the circulating bearing currents, as done in [14], the shield device is built by inserting a conductive material inside the motor with the aim of changing the machine parasitic capacitive couplings. In this context, regardless of using experimental measurements, as found in [1], [13] and [15] or computational simulations, as shown in [16] and [17], in general these works are concerned only with

evaluating the shield effectiveness to attenuate the undesired current. In addition, even the works that carried out a more complete investigation, also dealing with the shield influence on the motor operation, as in [12], [14] and [18], the impact on the motor temperature rise due to the shield presence is generally not accounted for. Thus, there are few studies that deal with a possible overheating inside the motor due to the presence of the shield, but they are related only to the EDM currents mitigation device. Besides, there is still no consensus about the shielding impact on the motor temperature distribution. In other words, there are some authors who believe that the shield has no influence on the temperature rise [19], whereas others state a motor overheating due to the shield presence [11].

In this context, the main objective of this work is to further analyze the shield device influence on the temperature distribution inside the motor slots. The generated losses in the stator and shield conductors are obtained from 2-D finite element analyses, and used as heat sources for the temperature calculation. The shield arrangement for the EMD current reduction, as well as the shield for circulating bearing current attenuation, are both addressed. Conclusions are drawn concerning the shield's impact not only on the temperature rise, but also with regards to the distribution of the losses in the stator conductors. In addition, the developed methodology can be used to accurately perform investigations on any motor, which greatly facilitates the analysis of the shield still in the design stage. Since the aim of such device is to prevent bearing failures and thus reduce the motor downtime, this paper is within the reliability scope and contributes with industry applications highly dependent on motor adjustable speed drives (ASD), such as the mining industry.

II. EDM AND CIRCULATNG BEARING CURRENTS DESCRIPTION

This section brings a brief review of the mechanisms related to the EDM and the circulating bearing currents. For more detailed information about these and the other inverter-induced bearing currents, the reference [20] should be consulted.

A. EDM Bearing Currents

At least two elements are fundamental for the EDM currents occurrence in the induction machine bearings. The first is the existence of a common mode voltage (CMV), which is naturally generated at the inverter output and applied to the winding motor terminals. The second concerns a circulation path, which is constituted by the distributed parasitic capacitive couplings that are formed inside the machine and are excited by the high frequency components of the common mode voltage. For a squirrel cage induction machine, there are three main capacitances to be cited: 1) The winding-to-frame capacitance (C_{wf}); 2) The winding-to-rotor capacitance (C_{wr}); 3) The rotor-to-frame capacitance (C_{rf}). The winding-to-rotor capacitive coupling is formed in the slot openings (C_{wr_sl}) as well as in the end-winding region (C_{wr_end}). The C_{rf} coupling is also formed in two regions: mainly at the air gap, between the stator and rotor cores (C_{rf}') and also at the motor bearings (C_b), since its lubrication film has insulating properties. Also, the stator iron stack is in contact with the stator frame (housing); thus, from the capacitances point of view, the stator core and frame form a single conductor.

These intrinsic capacitances can be represented as a capacitive voltage divider, as shown in Fig. 1. Thus, the common mode voltage is mirrored over the bearing, causing a shaft-to-frame voltage, as illustrated in Fig. 1 by V_b. Hence, if the V_b voltage exceeds a threshold value, the lubrication film breaks down and all the charge accumulated in the rotor-to-frame capacitance is discharged through the disrupted bearing, forming an EDM current.

The EDM currents can cause serious damage to the bearings. Smaller motors (few kW) are exposed to greater dangers, because the largest EDM bearing current densities are expected for these machines size [21].

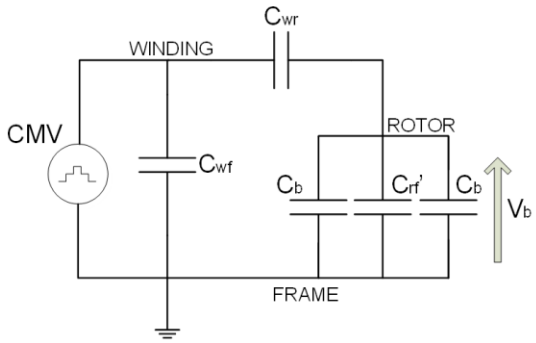

Fig. 1 Capacitive voltage divider for an induction machine

B. Circulating Bearing Currents

Among all stray capacitive couplings formed inside the induction machine, the stator winding-to-frame capacitance (C_{wf}) is predominant. Thus, for each switching event of the common mode voltage, almost all the common mode current (CMC) returns by the preferred path formed through the windings – stator core – frame. When passing through the core laminations, the CMC excites a high frequency magnetic flux around the rotor. This flux induces a voltage along the shaft ends and, if this voltage exceeds a threshold value to break the bearing insulating properties, a circulating current takes place. This current flows along the loop formed by the stator core – frame – non drive end shield – bearing – shaft – rotor core – shaft – bearing – drive end shield – frame – stator core, as shown in Fig 2.

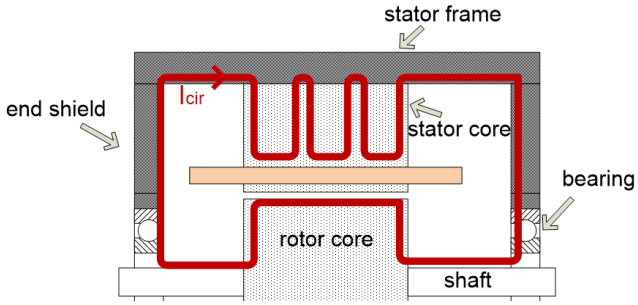

Fig 2. Circulating bearing current path inside the motor

As shown in [22], the circulating currents are more typical of larger machines (> 100 kW), because the end-to-end shaft voltage can easily exceed the bearing threshold level.

III. SHIELD ACTUATION EXPLANATION

For the mitigation of both the EDM current and the circulating current, the shielding device consists of a conductive material inserted inside the machine, with the aim of changing the motor intrinsic capacitive couplings. However, as will be shown in this section, the way in which the shield acts for each of these current types is very distinct.

A. Shield Device for EDM Current Attenuation

The main idea of using a shield device to reduce the EDM bearing currents is based on the reduction of the winding-to-rotor electrostatic coupling. This is done by covering the region between the stator conductors and the rotor with a conductive material (copper or aluminum), as illustrated in Fig. *3*. If this conductor is insulated from the other machine parts and properly grounded, it acts as a Faraday cage and protects the rotor from the external source. In this case, the rotor potential does not follow the common-mode voltage in the same way as in the situation without the shield, and therefore the possible EDM currents can be minimized.

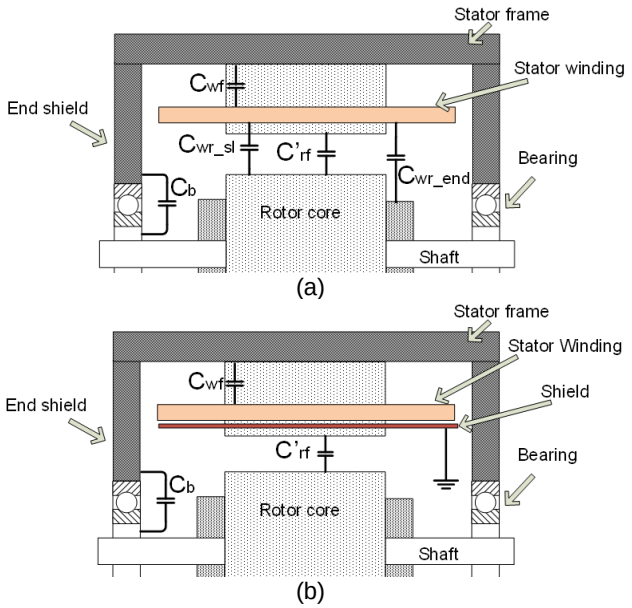

Fig. 3 Shielding actuation to eliminate the EDM currents: Capacitances distribution (a) without and (b) with the shield

B. Shield Device for Circulating Current Attenuation

To attenuate the circulating bearing currents, the shield device must be embedded into the stator slot, between the stator winding and the core surface. In this case, the winding-to-frame capacitance is reduced. Therefore, the portion of the common mode current that returns through the core laminations (I_{wf}) is decreased. As such, the shield guides the common mode current directly to the grounded point, avoiding the current circulation in the core laminations, as shown in Fig. 4. In this way, interdicting the current circulation in the stator core, the high-frequency magnetic flux around the rotor is attenuated. Thus, the end-to-end induced shaft voltage is reduced, mitigating the circulating currents.

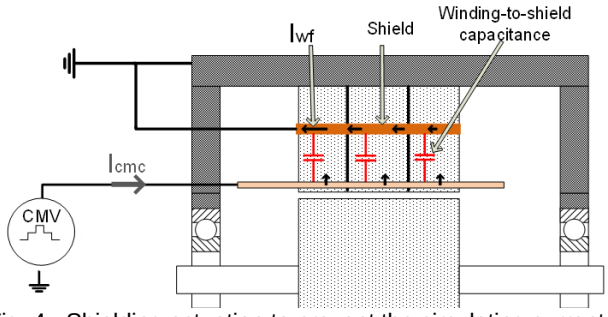

Fig. 4 - Shielding actuation to prevent the circulating currents

IV. THERMAL ANALYSIS OF THE STATOR SLOT

To evaluate the shield influence on the motor temperature, a 2-D finite element model was built to consider the heat flow in the stator slot. For such analysis, the steady state temperature (T) over a solution domain is obtained by solving (1).

$$-\nabla.(\lambda \nabla \mathrm{T}) = q_L \tag{1}$$

where

λ	thermal conductivity;
q_L	power loss density.

Despite the numerous heat sources inside an electric machine, this study only addresses the stator slots of a cage induction motor. Thus, only the average resistive losses inside the stator winding and the shield conductors are considered as heat sources. The loss calculation is performed by means of a second finite element model, as shown in Section V.

Two types of boundary conditions are used to solve the thermal problem. For the iron sides, the temperature is prescribed to zero at the boundaries. A convection boundary condition is applied at the slot opening by using (2),

$$\lambda \frac{\partial T}{\partial n} + h(T - T_0) \tag{2}$$

where

n	unit vector in the normal direction;
h	heat transfer coefficient;
T_0	air gap temperature.

The air gap temperature is also set to zero. Since the interest is to verify differences in the temperature distribution with and without the shield presence, the conditions defined above are reasonable [23].

Fig. 5 illustrates a stator core lamination, highlighting the solution domain with a dotted line and showing the defined boundary conditions.

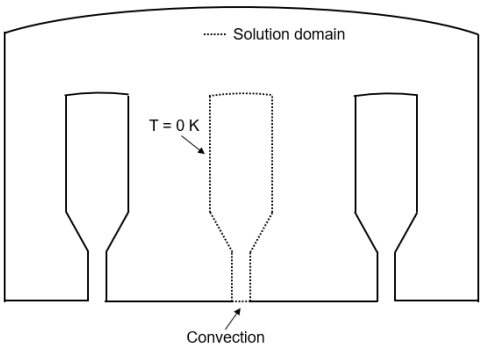

Fig. 5 Thermal problem domain: solution domain and boundary conditions

V. EDDY-CURRENT LOSS MODELLING

A time-stepping 2-D finite element model is used to determine the losses in the motor core region. The partial differential equation describing the magnetic vector potential (**A**) distribution in the region of interest is given by (3),

$$\nabla \times \frac{1}{\mu} \nabla \times \boldsymbol{A} + \sigma \frac{\partial \boldsymbol{A}}{\partial t} - \sigma \frac{u_c}{l_c} = 0 \qquad (3)$$

where

u_c electrical potential difference between the ends of a conductor;

l_c conductor length.

The stator winding is supplied by a PWM voltage source inverter. The PWM switching frequency is defined as 5 kHz and, for all cases of losses computation, the motors are considered to be operating at rated voltage and speed. The rotor end-ring is represented by circuit elements and the conductivity of the laminated core is negligible.

Solving the magnetic problem, the average loss density in the stator conductors and in the shield can be found. These values are then used as the heat source (input data) for the thermal model. More details about the loss calculation can be found in [10].

VI. INDUCTION MOTOR AND SHIELDING DEVICE SPECIFICATION

To perform the proposed investigation, two different motors are considered, whose main characteristics and evaluated shields are shown below.

A. Shield Device And 3 HP Motor Parameters – EDM Current Mitigation

For the EDM current mitigation analyses, a 3 HP, 380 V induction motor is used. It has a random-wound stator winding with three coils per group and two groups per phase, connected in parallel. The rotor is a squirrel cage type with closed slot and aluminum bars. The stator coils are built with enameled copper wires and the slot insulation material is a Dracon Mylar Dracon film (DMD). The main parameters of the induction motor used in the simulations are shown in Table I.

TABLE I
MAIN PARAMETERS OF THE 3 HP INDUCTION MOTOR

Rated Power	3 HP	Number of poles	4
Rated Voltage	380 V (YY)	Conductors/coil side	67
Rated Current	4.8 A	Coil sides/slot	1
Rated Speed	1735 rpm	Insulation Class	130 (B)

The shield consists of aluminum plates, with a cross-section of 2 mm by 0.5 mm, and extending the axial length along the slot, as shown in Fig. 6. To prevent an undesired contact with the core, the shield is surrounded by an insulating material.

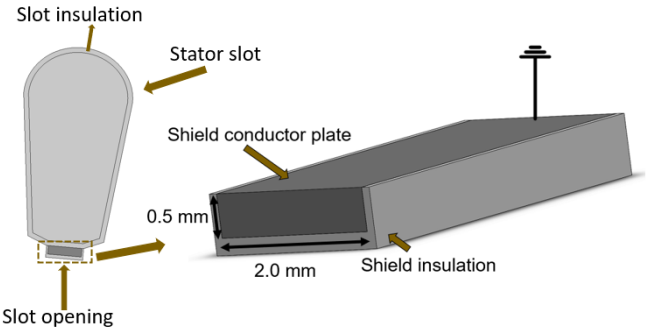

Fig. 6 Shield arrangement to mitigate the EDM currents

B. Shield Device And 250 HP Motor Parameters – Circulating Current Mitigation

For the circulating current mitigation analyses, a 250 HP, 2400 V induction motor is used. It has a form-wound stator winding with copper rectangular bars. All conductors of the same coil, as well as all the coils of the same phase, are connected in series. The slot insulation is formed by synthetic resins. The rotor is a squirrel cage type with semi-closed slot and copper bars. The main parameters of the induction motor used in the simulations are shown in Table II.

The shield is made of aluminum in an inverted “U” geometry, with 0.1 mm thick, an axial length matching the slot length and wide enough to cover the sides and bottom of the slot, as shown in Fig. 7. For the analyzed motor, the shield upper to bottom length is 48 mm.

TABLE II
MAIN PARAMETERS OF THE 250 HP INDUCTION MOTOR

Rated Power	250 HP	Number of poles	8
Rated Voltage	2400 V (YY)	Conductors/coil side	6
Rated Current	55.6 A	Coil sides/slot	2
Rated Speed	877 rpm	Insulation Class	155 (F)

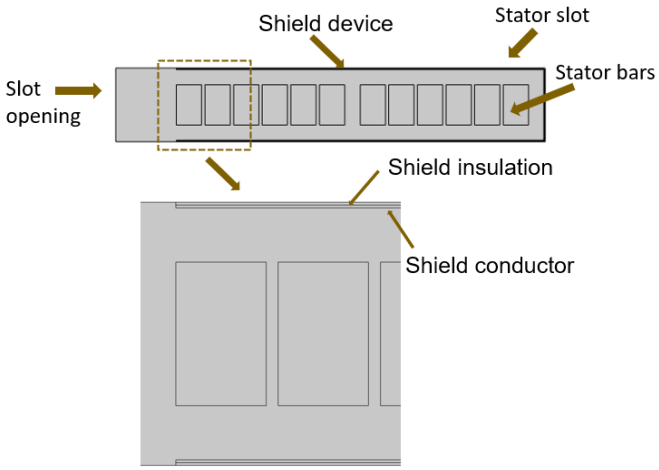

Fig. 7 Shield arrangement to mitigate the circulating currents

VII. RESULTS

In this section, the thermal analysis is performed according to the methodology presented in Section IV. The shielding device impact on the temperature rise of the stator slot for the two shielding arrangements is shown. Since the losses density are used as heat sources for the thermal model, the distribution of the losses in the stator winding and in the shielding device are also discussed for both the 3HP and 250 HP motors.

A. Shielding Device For EDM Currents Attenuation – 3 HP Motor Analysis

It was assumed for the 3 HP motor that the wires of the stator coils (random-wound coils) are thin enough to ignore the skin effect on each individual conductor. Thus, the current density in the stator coils is uniform, as shown in Fig. *8*(a). On the other hand, all the shield segments were individually modeled. Thus, the loss distribution in the shield plates is non-uniform, as shown in Fig. *8*(b).

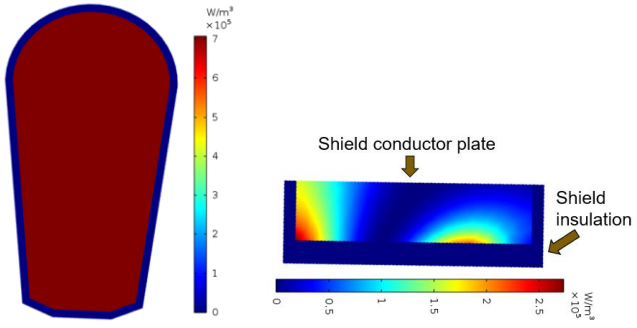

(a) (b)

Fig. 8 Density loss distribution inside the 3 HP motor: (a) Stator conductor; (b) Shield conductor

Fig. 9 shows the stator, rotor, shield and total losses for the 3 HP motor considering both situations, with and without the shield device. Due to the low value of the shield losses (approximately 2 W), its presence practically has no influence on the motor generated losses. Since the shield is positioned in the stator slot opening area, only a few flux lines cross through the shield plates, as shown in Fig. 10. Therefore, the eddy-current losses in the shield are negligible.

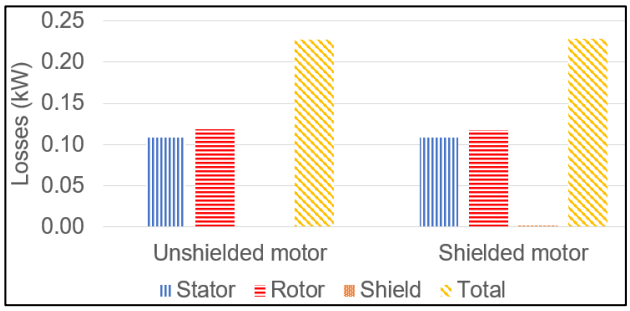

Fig. 9 Losses for the 3 HP motor with and without the shield presence

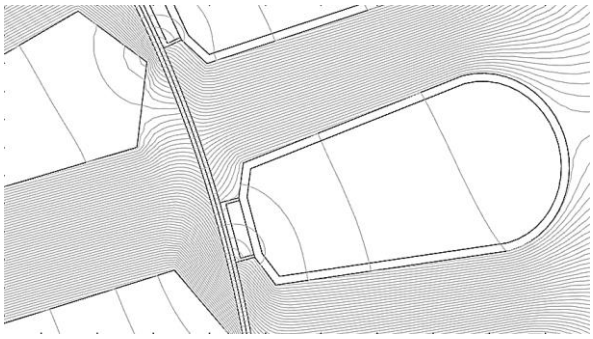

Fig. 10 Flux representation using magnetic equipotential lines

The average loss density of each conductor inside the slot is used to perform the thermal analysis. In other words, the heat sources considered as input data for the thermal model are the generated losses in the stator coils and in the shield device.

To better understand the origin of these heat sources, Fig. 11 shows the time variation of the average loss density in a coil side considering the original and the modified motor. Fig. 11 indicates the input value of 0.47 MW/m^3 that must be used in the thermal model to represent the generated heat in the coil. The same procedure is followed to obtain the value of 0.48 MW/m^3 for the generated heat in the shield. In this way, the heat sources that are used in the thermal analysis are summarized in Table III. It should be emphasized that the distortions present in the curves of Fig. 11 are related to the presence of high-frequency harmonic components in the magnetic flux inside the motor. Also, there is almost no difference in the stator losses with or without the shield presence.

The thermal conductivity of the insulation layer (Dracon Mylar Dracon – DMD) is 0.18 W/m·K and the heat transfer coefficient of the inside air is 35 W/m^2·K The thermal parameters are summarized in Table IV.

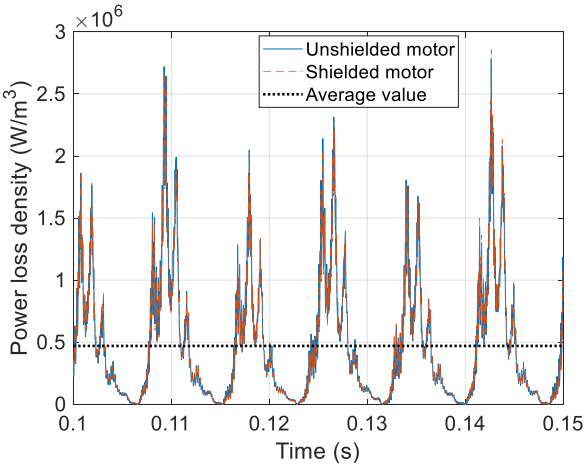

Fig. 11 Average power loss density time variation in a coil

TABLE III
HEAT SOURCES (INPUT DATA) FOR THE TEMPERATURE CALCULATION OF THE 3 HP MOTOR

Conductors	Power loss density (MW/m^3)	
	Unshielded motor	Shielded motor
Stator coil	0.47	0.47
Shield conductor	-	0.48

TABLE IV
THERMAL CONDUCTIVITIES OF THE MATERIALS USED IN THE THERMAL MODEL

Materials	Thermal conductivities (W/m.K)
Dracon Mylar Dracon – DMD 3 HP motor	0.18 [24]
Synthetic resins 250 HP motor	0.25 [25]
Copper	400
Aluminum	238

Using the thermal model described in Section IV, the temperature-rise distribution inside the 3 HP motor slot is obtained, as shown in Fig. 12. For the case without the shield, the stator slot opening is considered to be completely filled with insulating material. As can be seen in Fig. 12, in both cases the coil temperature rise is maintained at approximately 1.4 K. In face of such results, significant variations of the motor temperature distribution due to the shield presence are not expected, therefore avoiding the need to derate the machine.

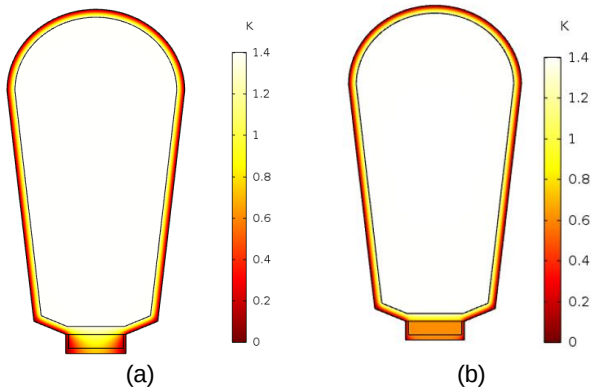

Fig. 12 Temperature-rise distribution in the stator slot: (a) Unshielded and (b) Shielded motor

B. Shielding Device For Circulating Currents Attenuation – 250 HP Motor Analysis

Since the circulating currents are more typical for larger motors, a 250 HP is used in the analysis. In this case, the stator winding is formed by copper bars (form-wound coils) and the coil turns are not thin enough to neglect the skin effect inside them. Therefore, to determine the losses in the 250 HP motor, all the stator conductors must be represented individually. Thus, it is possible to compute the non-uniformity of the loss distribution over the stator bars, as illustrated in Fig. 13.

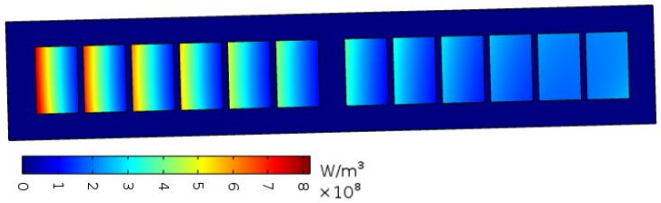

Fig. 13 Density loss distribution inside the stator bars of the 250 HP motor

Aside from the non-uniform distribution in each individual bar, Fig. 13 also shows that the bars closer to the air gap are subjected to greater losses. To illustrate this fact, Fig. 14 shows the losses in each bar of a single stator slot for both situations, with and without the shield. In Fig. 14, the index 1 represents the bar furthest from the air gap and the index 12 represents the closest one.

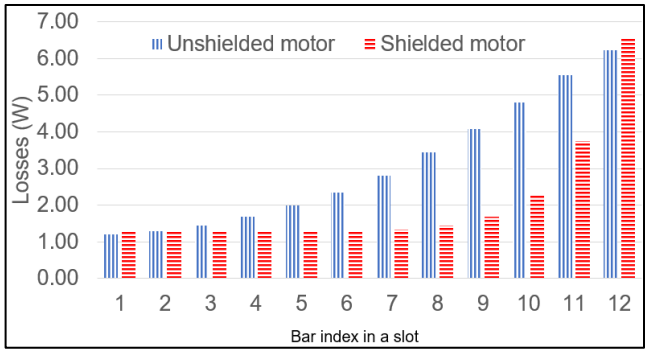

Fig. 14 Average loss distribution over the stator bars

Considering the slot region, the influence of both the fundamental main flux and the harmonic fluxes are more intense near the air gap, as stated in [26]. Thus, these flux components cause eddy current losses mainly in the conductors near the air gap. Therefore, some local overheating or hot spot can occur, putting the stator winding at risk. In other words, even if the global losses are at acceptable levels, these accentuated values of local losses can still damage the conductors. To avoid this problem, the motors could be equipped with magnetic wedges to redirect the magnetic flux in the slot opening area and protect the stator conductors, as shown in [23].

While the shielding device has no influence on the fundamental frequency flux, this is not true when considering the high-frequency harmonic fluxes associated with the PWM supply. Such harmonic fluxes flow mostly from one stator tooth to another, crossing almost all the shield plates, as illustrated by the field lines in Fig. 15. Thus, the induced currents in the shield generate an opposing magnetic field that mitigates these fluxes. To illustrate this phenomenon, Fig. 16 shows the field lines inside a slot, when considering the situations for the original and the modified motor, and a supply from a sinusoidal voltage source with a frequency of 5 kHz (which corresponds to the PWM switching frequency). Therefore, protecting the stator conductors from such harmonic fluxes, the shield presence reduces the eddy current losses in the stator winding, as illustrated in Fig. 17.

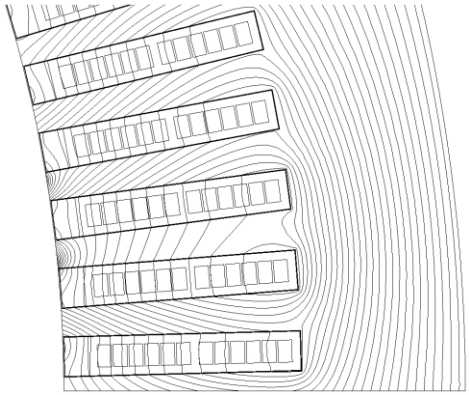

Fig. 15 High-frequency flux distribution at one instant of time. Simulation performed using a sinusoidal voltage source with a frequency of 5 kHz

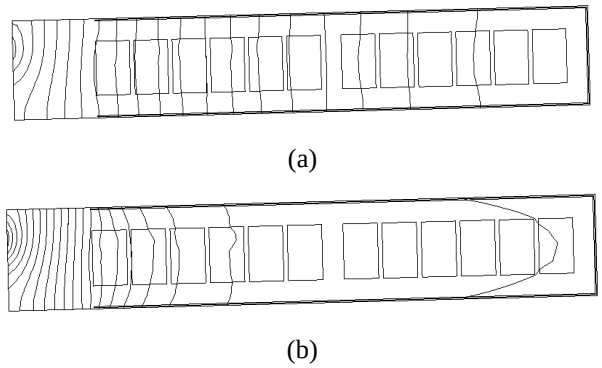

(a)

(b)

Fig. 16 Magnetic field lines inside the slot: (a) Without and (b) With the shielding device. Simulation performed using a sinusoidal voltage source with a frequency of 5 kHz

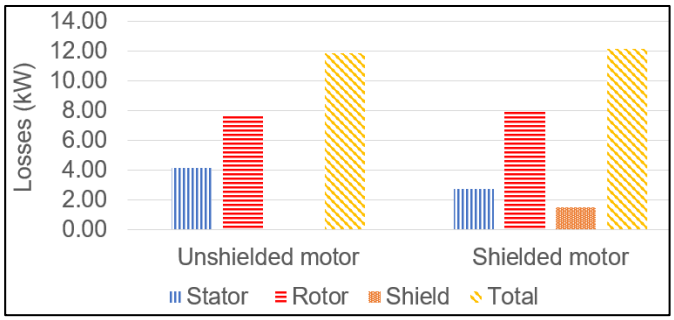

Fig. 17 Losses for the 250 HP motor with and without the shield presence

A further contribution to this discussion can be observed with Fig. 18, which illustrates the losses in each bar of a single slot for a sinusoidal supply with a frequency of 60 Hz. In this case, as there are no harmonic components imposed by the PWM supply, the shield has practically no influence on the stator winding losses.

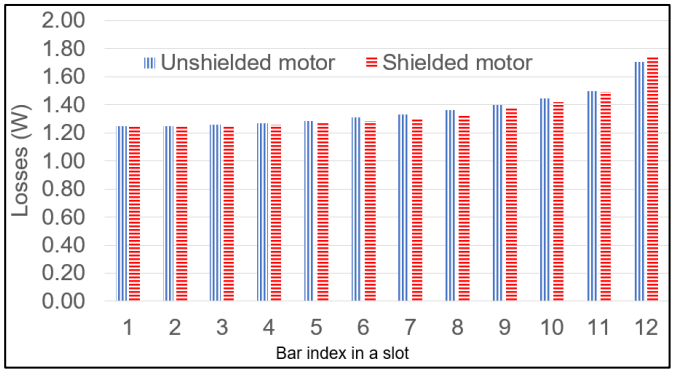

Fig. 18 Average loss distribution in the stator bars – Line-fed supply (60 Hz)

In the same way as determined for the 3 HP motor, the average loss density of each conductor inside the slot is employed to perform the thermal analysis. The thermal conductivity of the insulation layer (synthetic resins) is 0.25 W/m·K. Table IV and Table V show the main parameters used to calculate the temperature rise distribution.

TABLE V
HEAT SOURCES (INPUT DATA) FOR THE TEMPERATURE CALCULATION OF THE 250 HP MOTOR

Conductors	Power loss density (MW/m^3)	
	Unshielded motor	Shielded motor
Bar 1	0.30	0.32
Bar 2	0.32	0.32
Bar 3	0.36	0.32
Bar 4	0.42	0.32
Bar 5	0.50	0.32
Bar 6	0.59	0.33
Bar 7	0.70	0.34
Bar 8	0.86	0.36
Bar 9	1.02	0.42
Bar 10	1.20	0.57
Bar 11	1.39	0.94
Bar 12	1.56	1.64
Shield conductor	-	5.25

Erro! Fonte de referência não encontrada. shows the temperature rise distribution in a stator slot for the motor with and without the shielding device. Table VI presents the average and the maximum temperature values in the stator conductors for both situations. The maximum temperature of the stator bars drops from 21.6 K to 16.3 K considering the original and the modified motor, respectively. Also, the average temperature of these conductors decreases from 13.4 K (unshielded) to 8.6 K (shielded). Due to the attenuation in the stator bar losses, the results reveal that the shield presence can lead to a reduction of the maximum and average winding temperature.

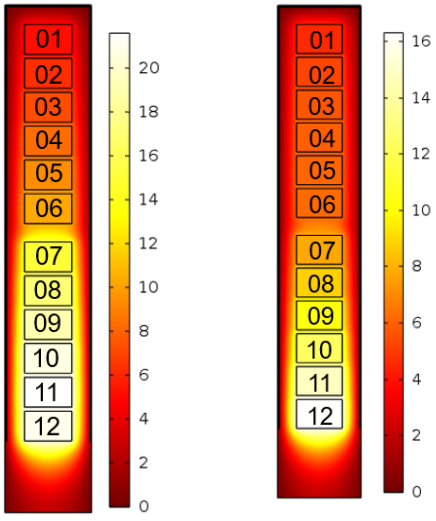

Fig. 19 Temperature-rise distribution in the stator slot: (a) Unshielded motor; (b) Shielded motor

TABLE VI
OVERVIEW OF THE STATOR BARS TEMPERATURE

Stator bars	Unshielded motor	Shielded motor
Maximum Temperature (K)	21.6	16.3
Average temperature (K)	13.4	8.7

VIII. CONCLUSIONS

This paper presented a thorough study on the thermal impact caused by the use of electrostatic shields for the inverter-induced bearing currents mitigation. Two shield configurations were analyzed, one used to attenuate the electrostatic discharge machining currents and the other to reduce the circulating bearing currents. From 2-D finite element models, the motor losses were calculated and used as heat sources to determine the temperature rise inside the stator slots.

A 3 HP induction motor was used to analyze the shield applied to the discharge currents attenuation. In this case, when the shield is positioned only at the slot opening, there is a reduced amount of magnetic flux crossing through the shield walls. Thus, the shield eddy-current losses are negligible and the shield impact on the temperature rise inside the motor slot can be ignored.

Regarding the circulating bearing current mitigation, a 250 HP motor was considered in the analysis. In this case, the results showed that the shield can attenuate the high-frequency harmonic fluxes associated with the PWM supply. In other words, the shield acts protecting the stator winding from such harmonic fluxes, reducing the eddy currents in the stator bars. Therefore, due to the decrease in the stator conductor losses, there is a reduction on the slot temperature.

It is important to stress that although the results were obtained only for two motor types, the methodology that was developed can be applied to evaluate the shielding device performance in any other machine.

IX. REFERENCES

[1] F. J. T. E. Ferreira, M. V. Cistelecan and A. T. d. Almeida, "Evaluation of Slot-Embedded Partial Electrostatic Shield for High-Frequency Bearing Current Mitigation in Inverter-Fed Induction Motors," *IEEE Transactions on Energy Conversion,* vol. 27, no. 2, pp. 382 - 390, Apr 2012.

[2] W. Tong, Mechanical Design of Electric Motors, CRC Press Taylor & Francis Group, 2014.

[3] R. d. S. Araújo, H. d. Paula, R. d. A. Rodrigues, L. M. R. Baccarini and A. V. Rocha, "Premature Wear and Recurring Bearing Failures in an Inverter-Driven Induction Motor—Part I: Investigation of the Problem," *IEEE Transactions on Industry Applications,* vol. 51, no. 6, pp. 4861 - 4867, Jul 2015.

[4] A. Romanenko, A. Muetze and J. Ahola, "Incipient Bearing Damage Monitoring of 940-h Variable Speed Drive System Operation," *IEEE Transactions on Energy Conversion,* vol. 32, no. 1, pp. 99 - 110, Oct 2016.

[5] P. L. Alger and H. W. Samson, "Shaft currents in electric machines," *Journal of the American Institute of Electrical Engineers,* vol. 42, no. 2, pp. 1325 - 1334, Dec 1923.

[6] C. Pearce, "Bearing Currents - Their Origin and Prevention," *The Electric Journal,* vol. 24, no. 8, pp. 372-376, 1927.

[7] R. F. Schiferl and M. J. Melfi, "Bearing current remediation options," *IEEE Industry Applications Magazine,* vol. 10, no. 4, pp. 40 - 50, Jul 2004.

[8] A. Muetze and H. W. Oh, "Design Aspects of Conductive Microfiber Rings for Shaft-Grounding Purposes," *IEEE Transactions on Industry Applications ,* vol. 44, no. 6, pp. 1749 - 1757, Nov. 2008.

[9] J. A. Oliver, G. Guerrero and J. Goldman, "Ceramic Bearings for Electric Motors: Eliminating Damage with New Materials," *IEEE Industry Applications Magazine ,* vol. 23, no. 6, pp. 14 - 20, Nov. 2017.

[10] M. T. A. Êvo and H. d. Paula, "Electrostatic shielding for bearings discharge currents attenuation: analysis of its effectiveness, losses and impact on the motor performance – a study for design guidelines," *IET Electric Power Applications ,* Vol. 14, no 6, pp. 1050-1059, Jun 2020.

[11] B. Bai, Y. Wang and X. Wang, "Suppression for Discharging Bearing Current in Variable-Frequency Motors Based on Electromagnetic Shielding Slot Wedge," *IEEE Transactions on Magnetics,* vol. 51, no. 11, Jun 2015.

[12] S. Gerber and R.-J. Wangi, "Reduction of Inverter-Induced Shaft Voltages Using Electrostatic Shielding," in *Southern African Universities Power Engineering Conference/Robotics and Mechatronics/Pattern Recognition Association of South Africa (SAUPEC/RobMech/PRASA)*, Bloemfontein, South Africa, May 2019.

[13] K. Vostrov, J. Pyrhönen, P. Lindh, M. Niemelä and J. Ahola, "Mitigation of Inverter-Induced Noncirculating Bearing Currents by Introducing Grounded Electrodes into Stator Slot Openings," *IEEE Transactions on Industrial Electronics,* vol. 68, no. 2, pp. 11752 - 11760, Dec. 2021.

[14] P. Mäki-Ontto and J. Luomi, "Bearing current prevention of converter-fed AC machines with a conductive shielding in stator slots," *IEEE International Electric Machines and Drives Conference, 2003. IEMDC'03,* vol. 1, pp. 274 - 278, Jun. 2003.

[15] O. Magdun, Y. Gemeinder and A. Binder, "Prevention of harmful EDM currents in inverter-fed AC machines by use of electrostatic shields in the stator winding overhang," in *36th Annual Conference on IEEE Industrial Electronics Society - IECON 2010*, Glendale, AZ, USA, Dec 2010.

[16] K. Vostrov, J. Pyrhönen, J. Ahola and M. Niemelä, "Non-circulating Bearing Currents Mitigation Approach Based on Machine Stator Design Options," in *XIII International Conference on Electrical Machines (ICEM)*, Oct 2018.

[17] K. Vostrov, J. Pyrhönen and J. Ahola, "Extension of slot-opening-embedded electrostatic shields in the region of the end-winding to effectively reduce parasitic capacitive coupling," in *IEEE International Electric Machines & Drives Conference (IEMDC)*, Hartford, CT, USA, Jun 2021.

[18] R. Liu, E. Yang, J. Chen and S. Niu, "Novel Bearing Current Suppression Approach in Doubly-Fed Induction Generators," *IEEE Access ,* vol. 7, pp. 171525 - 171532, Nov 2019.

[19] D. F. Busse, J. M. Erdman, R. J. Kerkman, D. W. Schlegel and G. L. Skibinski, "An evaluation of the electrostatic shielded induction motor: a solution for rotor shaft voltage buildup and bearing current," *IEEE Transactions on Industry Applications,* vol. 33, no. 6, pp. 1563 - 1570, Nov. 1997.

[20] M. T. A. Êvo, A. M. Alzamora, I. O. Zaparoli and H. d. Paula, "Inverter-induced bearing currents – A thorough study of the cause-and-effect chains," in *IEEE Industry Applications Society Annual Meeting (IAS)*, Vancouver, BC, Canada, Oct 2021.

[21] A. Binder and A. Muetze, "Scaling Effects of Inverter-Induced Bearing Currents in AC Machines," *IEEE Transactions on Industry Applications,* vol. 44, no. 3, pp. 769 - 776, May 2008.

[22] A. Muetze and A. Binder, "Calculation of Circulating Bearing Currents in Machines of Inverter-Based Drive Systems," *IEEE Transactions on Industrial Electronics,* vol. 5, no. 2, pp. 932 - 938, Apr 2007.

[23] M. J. Islam, H. V. Khang, A.-K. Repo and A. Arkkio, "Eddy-Current Loss and Temperature Rise in the Form-Wound Stator Winding of an Inverter-Fed Cage Induction Motor," *IEEE Transactions on Magnetics,* vol. 46, no. 8, pp. 3413 - 3416, Aug 2010.

[24] L. Marackova, V. Melcova, J. Samek and O. Zmeskal, "Thermal Properties of Electro Insulating Paper," *Materials Science Forum,* pp. 25-30, 27 May 2019.

[25] T. A. Lipo, Introduction to ac machine design, New Jersey: John Wiley & Sons, Inc, 2017.

[26] M. Islam and A. Arkkio, "Effects of pulse-width-modulated supply voltage on eddy currents in the form-wound stator winding of a cage induction motor," *IET Electric Power Applications,* vol. 3, no. 1, pp. 50 - 58, Jan. 2009.

X. VITAE

Marco Tulio Alves Êvo was born in Patos de Minas, Brazil, on November 13, 1987. He received the B.Sc., M.Sc., and Ph.D degrees in electrical engineering from the e Federal University of Minas Gerais, Belo Horizonte, MG, Brazil in 2011, 2014, and 2020, respectively. He is currently a professor of electrical engineering with the e Federal University of São João del Rei del Rei, MG, Brazil. He has been teaching courses on electrical machines since 2014. His main interests include motor drives, and electromagnetic compatibility.

Arismar M. G. Júnior received the B.Sc. and M.Sc. degrees in Electrical Engineering from Federal University of São João del Rei (UFSJ, 2011 and 2013, respectively) and the Ph.D. degree in Electrical Engineering from Federal University of Minas Gerais

(UFMG, 2018). He was a Postdoctoral Research Fellow with the Department of Electrical and Computer Engineering, School of Engineering of São Carlos, University of São Paulo, Brazil (USP, 2020). His research interests include Electrical Machines, Signal Processing, Optimization and Machine Learning Methods.

Caio Eduardo Silva received the B.Sc. degree in Electrical Engineering from Federal University of São João del-Rei (UFSJ), in 2012, and the M.Sc. degree in Electrical Engineering on the Graduate Program in Electrical Engineering of UFSJ / CEFETMG, from UFSJ, in 2015. Since 2014, he has held the position of Electrical Engineer in the Projects and Works Division of UFSJ. Currently is a Ph.D. student the Graduate Program in Electrical Engineering of the Federal University of Uberlândia (UFU). His research interests focus on Motor Drives, Multilevel Inverters, Reliability based on Physics of Failure (PoF), Direct Current Transmission and Electric Drives.

Hélder de Paula was born in Uberlândia, Brazil, on December'75. He received the B.Sc., M.Sc. and Ph.D. degrees in Electrical Engineering from the Federal University of Uberlândia (UFU) in 1998, 2001, and 2005, respectively. From July'06 until November'17 he was with the Electrical Engineering Department of the Federal University of Minas Gerais (UFMG); since then he is a member of the Faculty of Electrical Engineering of UFU. Since April'21 he's been the Vice Chair of the Mining Committee of the Industry Applications Society of the IEEE. His main interests are motor drives, power quality, reliability and underground power transmission.